Arch. Mech., **58**, 6, pp. 543–573, Warszawa 2006

Shock wave smearing by wall perforation*)

P. DOERFFER, O. SZULC

IMP PAN,
Fiszera 14, PL-80 952 Gdańsk, Poland

Normal shock wave, terminating a local supersonic area on an airfoil, not only limits aerodynamic performance but also becomes a significant source of a high-speed impulsive noise on the rotor blade of a helicopter. It is proposed to apply passive control to disintegrate the shock wave by smearing pressure gradients created by the shock. Details of the flow structure obtained by this method are studied numerically. A new boundary condition of a perforated wall is verified against experimental data for a passive control of the shock wave in a channel flow and on an airfoil. This method of shock wave disintegration is proven to work for internal flows in transonic nozzles and appears to be effective for transonic airfoils as well. The substitution of a shock wave by a gradual compression changes completely the source of the high-speed impulsive noise and bears potential of its reduction.

Key words: transonic flows, shock wave boundary layer interaction, passive control.

1. Introduction

Passive shock wave – boundary layer interaction control using perforated surfaces was intensively investigated in research projects Euroshock I and II [1, 2]. The main aim of this research was to improve flow conditions on an airfoil at transonic Mach numbers. It was proven that under some specific conditions, application of a short perforation ($< 10\%$ of the chord length) resulted in improved performance of an airfoil, allowing higher free stream Mach numbers without any penalty, neither in lift nor in drag.

Another attitude towards airfoil performance has to be taken into account with respect to the rotor blade of a helicopter in high-speed forward flight and in high-speed hover conditions. Here, the most negative effect is the generation of a shock wave, which is responsible for a high-speed impulsive noise. Prevention of this shock generation would be of a very high priority in the development of the helicopter rotor. However, to disintegrate the shock, a relatively long perforation ($\sim 50\%$ of the chord length) has to be correctly located under the shock. It must have a large impact on the aerodynamic performance.

---

*)Paper presented at the 17–th Conference on Fluid Mechanics held in Bełchatów, September 17–21, 2006.

2. Passive control of the shock wave by wall perforation – B/D transpiration law [4]

A new boundary condition was implemented into the SPARC [3] code allowing modelling of the passive control by wall perforation (Figs. 1 and 2). The transpiration model describes a relation between the pressure difference over the perforated plate and the induced mass flow rate.

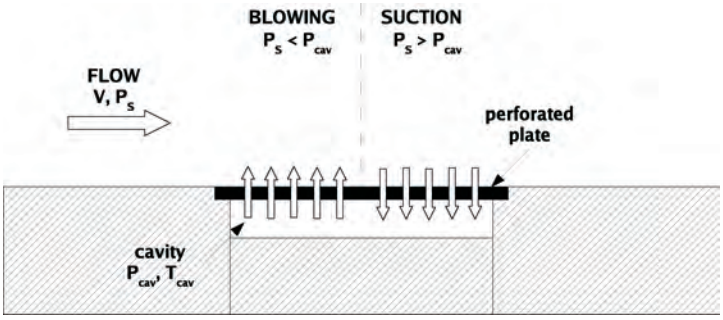

FIG. 1. Blowing and suction through a perforated plate.

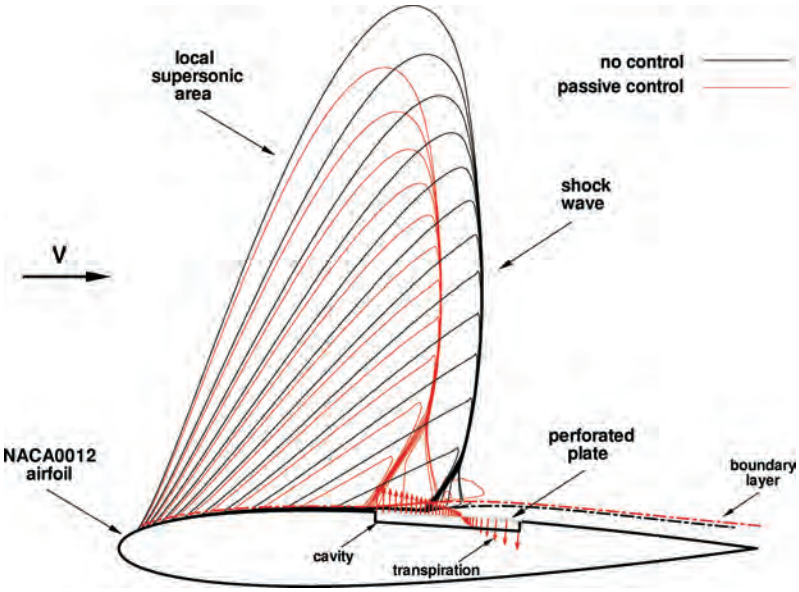

FIG. 2. Passive control of the shock wave on an airfoil.

Experiments have proven that pressure in the cavity volume P_{cav} may be considered as a constant. Having a pressure in the main stream P_{s} one may determine the pressure difference over the plate $\Delta P = P_{\mathrm{s}} - P_{\mathrm{cav}}$ along the perforated wall.

Using B/D formulation [4, 5]:

$$M_h = 1.2 \left(\frac{\Delta P}{P_0}\right)^{0.55} \tag{2.1}$$

one may determine an effective Mach number in a single hole M_h and knowing the porosity of the plate p – the corresponding mass flow rate. P_0 is the stagnation pressure of the tangential stream at the inlet side of the perforated plate. Experiments have shown that choking of the flow in the perforation holes takes place at rather low effective Mach number $M_h = 0.57$, which is a limiter for the boundary condition. Having these data an effective value of the transpiration velocity V_t normal to the wall may be determined and applied in the numerical code as a boundary condition.

In the standard no-slip wall boundary condition both velocity components (tangential and normal) and eddy viscosity are set to zero at the wall. For zero heat flux condition, pressure and density are extrapolated to the wall from the interior of the computational domain. The construction of the transpiration flow boundary condition is very similar, but includes non-zero normal velocity component of velocity V_t at the wall, which is calculated from the B/D law.

The passive behaviour of the boundary condition clearly indicates a need for an automatic adjustment of the cavity pressure value P_{cav} during each time step of the numerical scheme. It results in an instantaneous zero total mass flow rate through the perforated plate. Stagnation temperature T_{cav} in the passive control system is assumed constant and equal to the total temperature in the free stream.

Often the perforated plates display different flow characteristics depending on the flow direction. Therefore, in our boundary condition, a perforated plate may have different aerodynamic porosity p value dependent on the direction of the transpiration flow (suction or blowing).

3. Numerical method of solution – SPARC code

The present investigation was carried out with a standard cell-centered block-structured parallel CFD code SPARC [3] developed in a group of F. Magagnato at the University of Karlsruhe. This code solves numerically the compressible, mass-weighted, Reynolds-averaged Navier–Stokes equations with several turbulence models. The one-equation, low-Reynolds turbulence model of Spalart–Allmaras proved to be efficient in prediction of a strong shock wave – turbulent boundary layer interaction in presence of a transpiration flow.

The algorithm uses a semi-discrete approach, utilizing a finite-volume, density-based formulation for spatial discretisation (central scheme, 2-nd order of accuracy) and an explicit Runge–Kutta-type method for integration in time. In order

to increase the convergence rate, the local time stepping and the implicit residual averaging techniques are included in the explicit approach. Additionally, the full multigrid strategy with V-cycles is used. To damp numerical oscillations, the artificial dissipation SLIP scheme is incorporated into the code.

4. Disintegration of the shock wave in a curved channel

The validation procedure of a new boundary condition of a perforated wall was conducted for a transonic flow in the curved channel equipped with a 72 mm long perforation (nominal porosity $p = 8.2\%$) located under the shock. These computations were designed not only to validate the correctness of the implementation, but also to prove that the experimental disintegration of the normal shock wave by perforation is well reflected by the numerics. Additionally, structure of the interaction in the curved channel (local supersonic region terminated by a shock wave) is very similar to the shock-boundary layer interaction on an airfoil, which is of the highest priority in the current research.

At the beginning of nineties, BOHNING and BRAUN [6] have shown experimentally that with a special passive cavity length and location it is possible to substitute a normal shock wave, terminating a local supersonic area, by a disturbance reflecting between the sonic line and the wall.

The experimental interferogram photographs [6] showing iso-density lines of a flow-field near the curved wall of the nozzle are presented in Fig. 3 and Fig. 4. The flow direction is from left to right. A normal shock wave (Fig. 3), terminating a local supersonic area, is quite strong leading nearly to incipient separation, with shock upstream Mach number of $M = 1.26$ commonly present on transonic airfoils, where large pressure gradient becomes a source of noise.

FIG. 3. Isolines of density
Experiment, $Ma = 1.26$, no control.

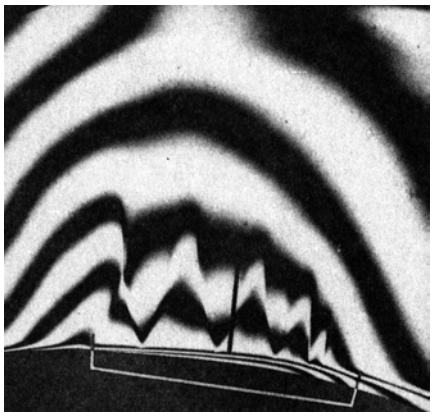

FIG. 4. Isolines of density
Experiment, $Ma = 1.26$, passive control.

The idea was to introduce a passive control method in which a cavity covered by a perforated plate is located under the shock wave. The beginning of the cavity was located sufficiently far upstream, so that the disturbance induced by the beginning of bleeding interferes with the sonic line (Fig. 4). In such a case, the shock wave disappears and is substituted by a disturbance reflecting between the sonic line and the wall.

Numerical simulations were performed using two- and three-dimensional computational meshes. A two-dimensional mesh consisted of 450 000 volumes, allowing very sharp definition of the shocks in the interaction region above the cavity location (Fig. 5). A three-dimensional mesh consisting of 2.8 million volumes allowed correct capturing of the pressure level in the channel due to the presence of sidewall boundary layers.

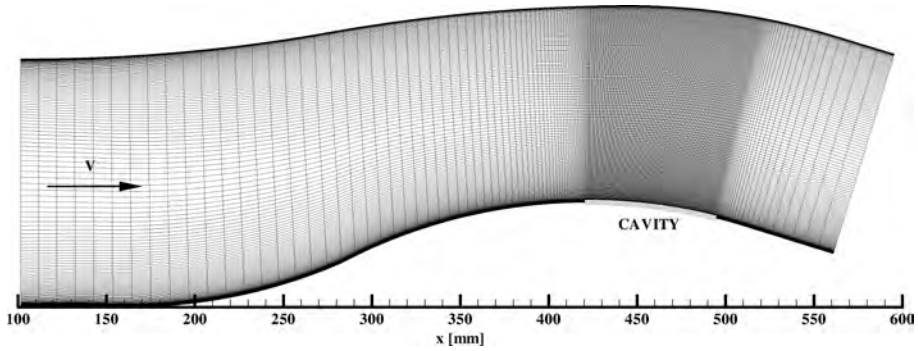

FIG. 5. Curved channel computational mesh (every second line drawn).

The computed density field was processed so that it shows the fringe pattern similar to the experimental interferogram pictures allowing comparison with the wind tunnel data (Figs. 6 and 7). The disintegration of the strong, normal shock wave and substitution by a weaker compression wave reflecting between the wall and the sonic line, is very well reproduced by the numerics.

FIG. 6. Isolines of density
2D CFD, $Ma = 1.26$, no control.

FIG. 7. Isolines of density
2D CFD, $Ma = 1.26$, passive control.

It is worth mentioning that application of a very dense two-dimensional mesh enabled a very sharp definition of the shocks, without any special shock-capturing scheme or automatic mesh adaptation. On the other hand, a two-dimensional simulation does not reproduce the existence of the sidewall boundary layers present in the experiment. It results in a small deviation of the pressure level at the wall of the nozzle in comparison with the experimental data (Figs. 8 and 9). The full three-dimensional computation predicts the pressure distribution very well, even in presence of a perforation.

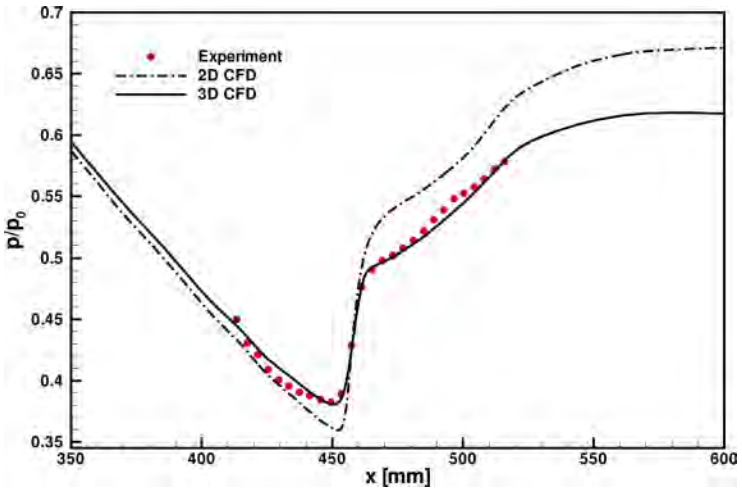

FIG. 8. Static pressure at the wall, $Ma = 1.26$, no control.

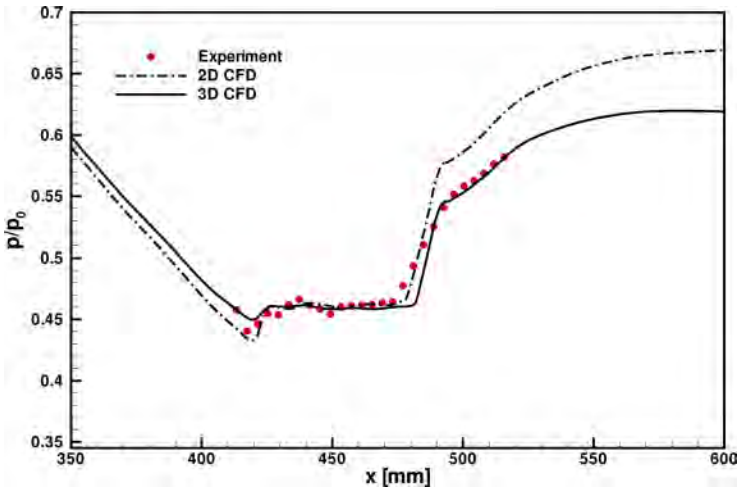

FIG. 9. Static pressure at the wall, $Ma = 1.26$, passive control.

The pressure jump at the wall, associated with the shock, is significantly reduced by the presence of perforation. The real pressure disturbance, which exists in the flow, is located some distance from the wall, giving major contribution to a high-speed impulsive noise generation. The strong pressure jump above the wall caused by the normal shock wave has been substituted by a weak pressure fluctuation of much smaller amplitude when passive control is applied (Fig. 10).

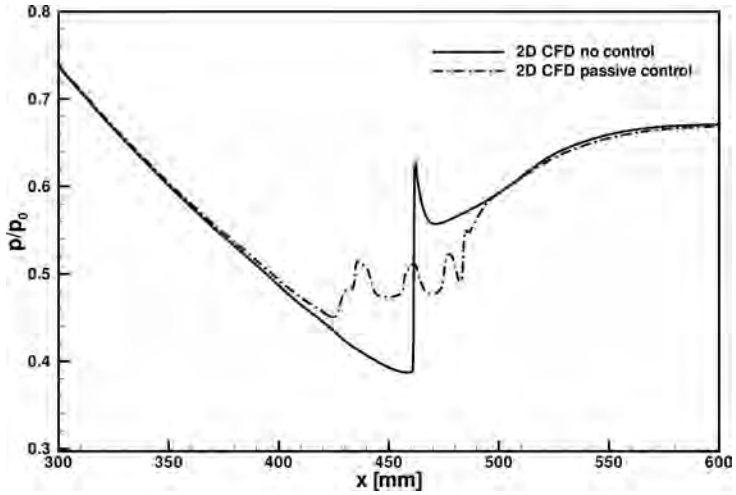

FIG. 10. Static pressure 10 mm above the wall, 2D CFD, $Ma = 1.26$.

It was proven that our numerical method is capable of predicting passive control by wall perforation in the configuration, leading to the elimination of the strong and steep pressure jump induced by a shock wave.

5. Transonic flow past the NACA 0012 airfoil – validation of the numerical method

Unfortunately, the experimental data showing shock disintegration by perforation are available only for the internal flow in a curved nozzle. The next level is to investigate in details the proposed method of shock disintegration for an airfoil flow, being a step forward towards simulation of the helicopter rotor. However, before applying perforation, it is necessary to assess the ability of the code to predict transonic flows past a popular, classical NACA 0012 profile. The NACA 0012 is the most comprehensively tested airfoil in wind tunnels in the history of aviation, having the largest available experimental database.

Three transonic test cases computed during the Viscous Transonic Airfoil Workshop [7] were calculated and compared with the experimental data of HARRIS [8]. All flow parameters were chosen to obtain a Reynolds number of 9 million, which is comparable with a maximum Reynolds numbers achievable during the flight of a helicopter. In addition, the Mach number and angle of attack were chosen to reflect real conditions on the rotor blade. The laminar-turbulent transition was fixed at 5% of the chord in both experiment and computations. All test cases were simulated using a two-dimensional mesh divided into 350 000 volumes (Fig. 11).

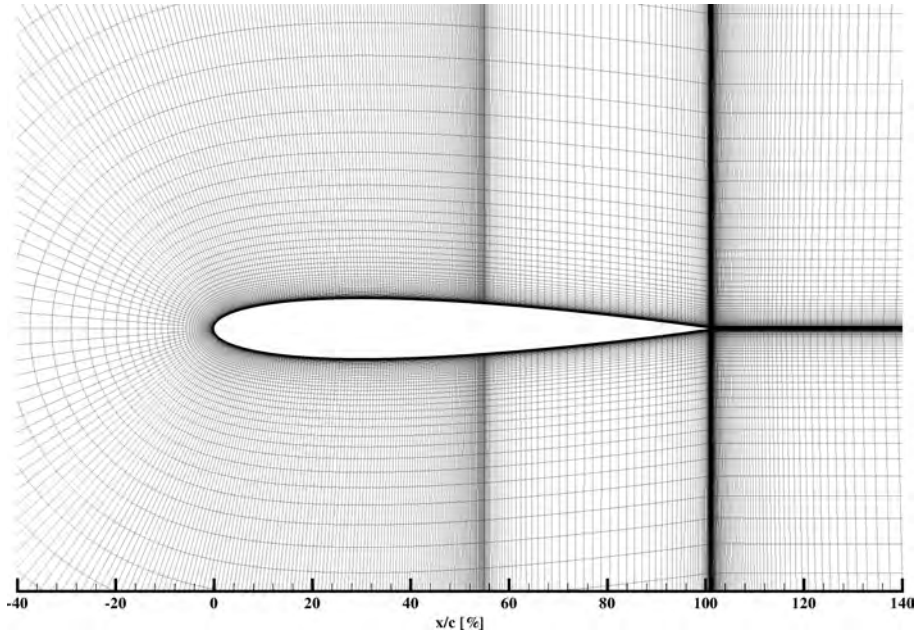

FIG. 11. NACA 0012 computational mesh (every second line drawn).

The first test case is a low speed ($Ma = 0.55$) and high angle of attack ($\alpha = 8.34°$) flow. These flow conditions are common for the retreating blade of a helicopter rotor in forward flight. Here a high angle of attack (near stall) leads to a very strong acceleration of the flow around the leading edge of the airfoil and creation of a shock wave near 10% of the chord ,with a maximum supersonic Mach number equal to 1.6 (Fig. 12).

The shock is strong enough to lead to a small flow separation predicted also by computation. A comparison of the experimental C_P distribution at the wall with a CFD result gives an acceptable agreement (Fig. 13). In addition, aerodynamic coefficients summarized in Table 1 coincide well enough with experimental

data. The normal force coefficient C_n is under predicted by 5%. The drag force coefficient C_d is over predicted by 37%, while the pitching moment coefficient C_m is over predicted by 12%.

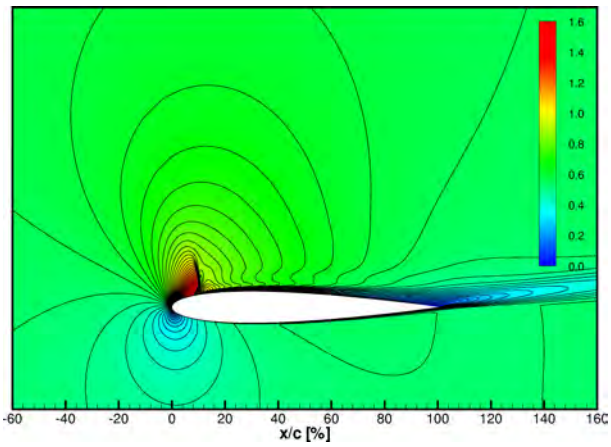

FIG. 12. Contour map of Mach number, CFD, $Ma = 0.55$, $Re = 9$ million, $\alpha = 8.34°$, $tr = 5\%$.

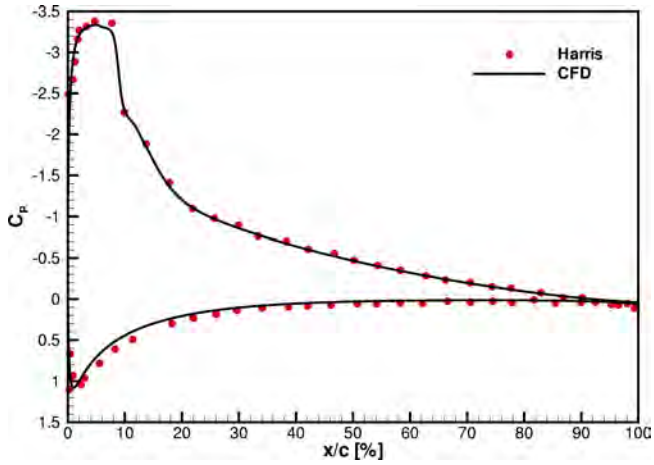

FIG. 13. C_p distribution at the wall, $Ma = 0.55$, $Re = 9$ million, $\alpha = 8.34°$, $tr = 5\%$.

Table 1. NACA 0012, $Ma = 0.55$, $Re = 9$ million, $\alpha = 8.34°$, $tr = 5$ %.

	α [°]	α_{corr} [°]	C_n	C_d	C_m
Harris	9.86	8.34	0.983	0.0253	0.033
CFD	–	8.34	0.931	0.0347	0.037

A second test case is a medium speed ($Ma = 0.7$) and low angle of attack ($\alpha = 1.49°$) flow. Here a low angle of attack and a relatively low Mach number result in a slight acceleration of the flow up to the maximum Mach number equal to 1.1 (Fig. 14). For this low supersonic flow, a barely seen shock wave is starting to develop near 20% of the chord.

A comparison of the experimental C_P distribution at the wall with a CFD result gives acceptable agreement (Fig. 15). In addition, the aerodynamic coefficients summarized in Table 2 compare well enough with the experimental data. The normal force coefficient C_n is over predicted by 0.5%. The drag force coefficient C_d is under predicted by 18%, while the pitching moment coefficient C_m is under predicted by 10%.

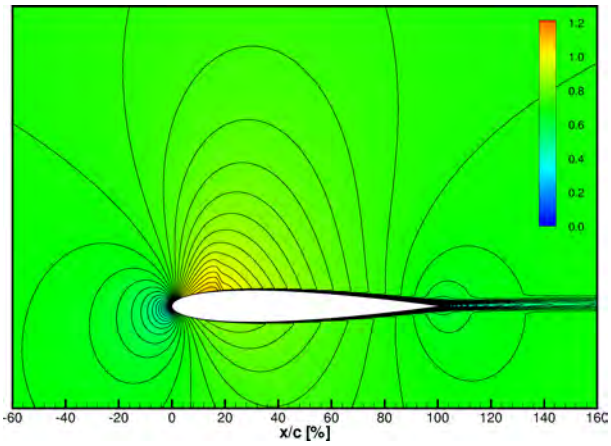

FIG. 14. Contour map of Mach number, CFD, $Ma = 0.7$, $Re = 9$ million, $\alpha = 1.49°$, $tr = 5\%$.

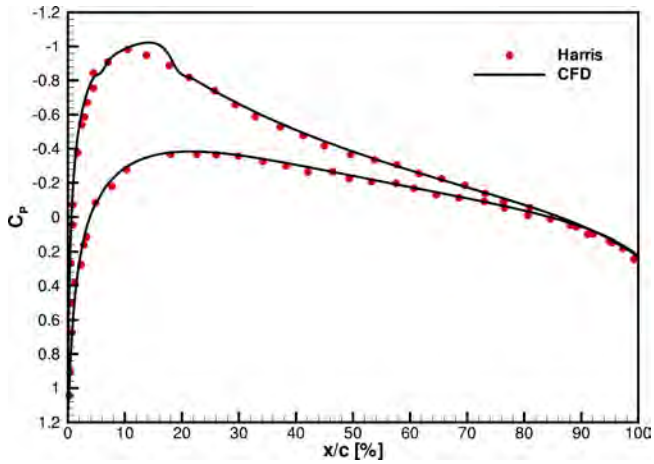

FIG. 15. C_p distribution at the wall, $Ma = 0.7$, $Re = 9$ million, $\alpha = 1.49°$, $tr = 5\%$.

Table 2. NACA 0012, $Ma = 0.7$, $Re = 9$ million, $\alpha = 1.49°$, $tr = 5\%$.

	$\alpha[°]$	α_{corr} [°]	C_n	C_d	C_m
Harris	1.86	1.49	0.241	0.0079	0.005
CFD	–	1.49	0.242	0.0065	0.0045

The last test case is a high speed ($Ma = 0.8$) and moderate angle of attack ($\alpha = 2.26°$) flow. These flow conditions are typical for the advancing blade of a helicopter rotor. The formation of a large supersonic region on this blade is responsible for a very strong high-speed impulsive noise. A high free-stream Mach number leads to a strong acceleration of the flow around the airfoil and creation of a large supersonic region with a shock wave located near 50% of the chord (Fig. 16). The maximum Mach number is equal to 1.4.

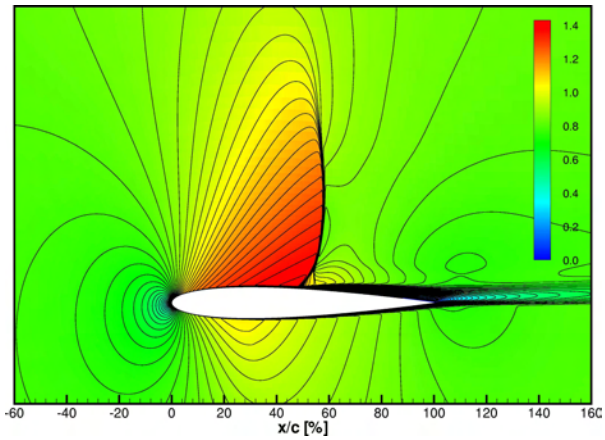

FIG. 16. Contour map of Mach number, CFD, $Ma = 0.8$, $Re = 9$ million, $\alpha = 2.26°$, $tr = 5\%$.

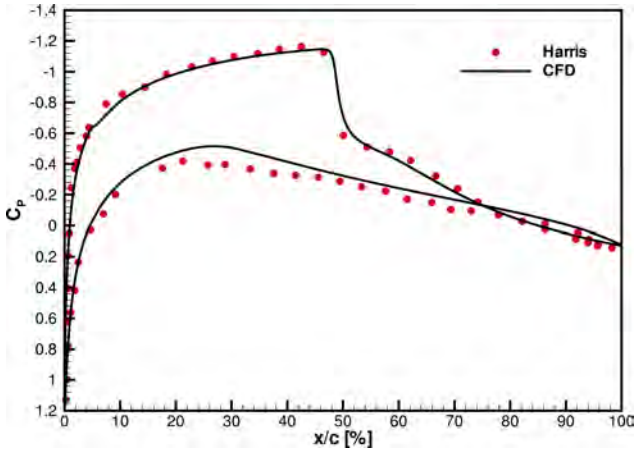

FIG. 17. C_p distribution at the wall, $Ma = 0.8$, $Re = 9$ million, $\alpha = 2.26°$, $tr = 5\%$.

The shock is strong enough to lead to a flow separation extended to the trailing edge, predicted also by the computation. A comparison of the experimental C_P distribution at the wall with a CFD result gives an acceptable agreement (Fig. 17). It is worth to notice that a proper shock position in the calculation is difficult to obtain and very sensitive to the correct prediction of the separation area downstream of the shock. In addition, the aerodynamic coefficients summarized in Table 3 compare well enough with the experimental data. The normal force coefficient C_n is under predicted by 16%. The drag force coefficient C_d is over predicted by 4%, while the pitching moment coefficient C_m is under the predicted by 30%.

Table 3. NACA 0012, $Ma = 0.8$, $Re = 9$ million, $\alpha = 2.26°$, $tr = 5\%$.

	$\alpha\,[°]$	$\alpha_{\mathrm{corr}}\,[°]$	C_n	C_d	C_m
Harris	2.86	2.26	0.390	0.0331	−0.016
CFD	–	2.26	0.326	0.0345	−0.011

Presented results may be considered as an improvement in comparison with the Viscous Transonic Airfoil Workshop predictions [7]. The current computations predict correctly shock location and flow separation, just downstream of the shock that was missing in the Workshop results. It is clearly visible in the distribution of a pressure coefficient C_p at the surface of the profile. To apply the perforation boundary condition it is necessary to predict both, the shock location and pressure distribution at the wall just upstream and downstream of the shock, especially well. The calculation of the transpiration velocity is based on the pressure difference between the flow and the cavity. Errors in the computed pressure above the wall will be reflected in a wrong transpiration intensity and can lead to poor, unphysical results.

The largest negative effect on the flow (and on the acoustic noise) appears for typical flow conditions of $Ma = 0.8$ and $Re = 9$ million presented during Viscous Transonic Airfoil Workshop as a third test case. Similar strong shock wave - boundary layer interaction leading to separation occurs typically on a helicopter blade. Because it is our aim to disintegrate the shock for these particular flow conditions, another extension of the validation is performed – a whole polar for $Ma = 0.8$, $Re = 9$ million and transition fixed at 5% c is computed and verified against the most common experimental data of HARRIS [8], LADSON [9, 10] and MINECK [11]. The experimental data of Harris is the most often used in validations of the CFD codes and is available in an uncorrected and linearly corrected form for wall interference effects. The data of Ladson and Mineck is used without any corrections. It is evident that transonic experiment is very sensitive, for these flow conditions, resulting in a significant scatter of the measured data.

The comparison of the computed and measured aerodynamic characteristics of the NACA 0012 profile with an inflow Mach number of $Ma = 0.8$, a Reynolds number of $Re = 9$ million and an angle of attack between $\alpha = -0.109°$ and $\alpha = 4.76°$ is presented in Figs. 18, 19, 20 and 21. The experimental data were obtained using fixed location of laminar – turbulent transition at 5% c, while the computations are fully turbulent. Satisfactory agreement is obtained for the normal force coefficient C_n, especially with the data of Ladson and Mineck and even for higher angles of attack (Fig. 18). In the real flow above $\alpha = 4°$ or even earlier, a very strong shock oscillation develops resulting in buffeting.

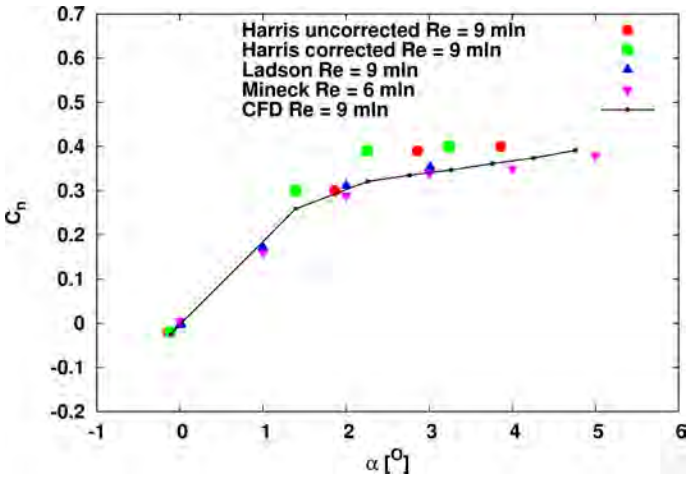

FIG. 18. Normal force coefficient, $Ma = 0.8$, $Re = 9$ million, $tr = 5\%$, CFD fully turbulent.

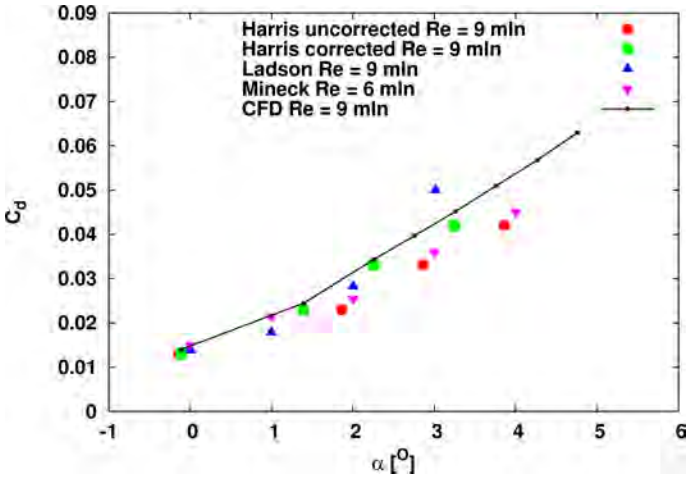

FIG. 19. Drag force coefficient, $Ma = 0.8$, $Re = 9$ million, $tr = 5\%$, CFD fully turbulent.

The drag force coefficient C_d seems to agree satisfactorily with the experiments, especially with corrected data of Harris (Fig. 19). CFD tends to overestimate the drag force slightly with increasing angle of attack.

The most difficult to obtain is a good agreement with the experimental values of the pitching moment coefficient C_m. It is extremely sensitive to correct shock position and a proper distribution of the loading on the surface of the profile. Even with correct total force coefficients (C_n and C_d) it is not enough to get a proper C_m value. In this respect, the presented comparison is very satisfactory reflecting the shape of the experimental data with small underestimation near the middle of the range of angle of attack (Fig. 20).

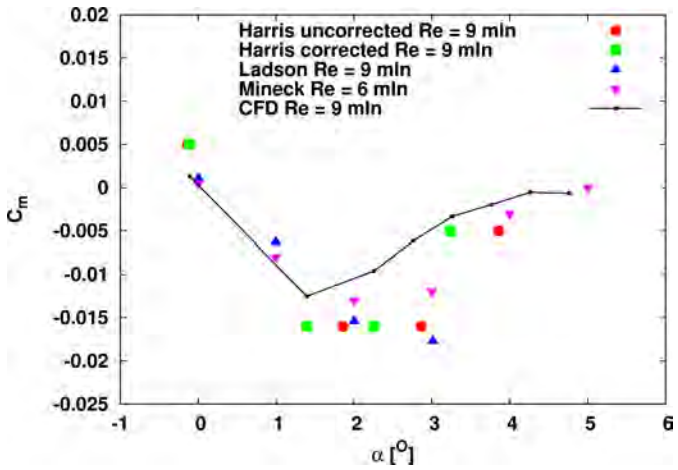

FIG. 20. Pitching moment coefficient, $Ma = 0.8$, $Re = 9$ million, $tr = 5\%$, CFD fully turbulent.

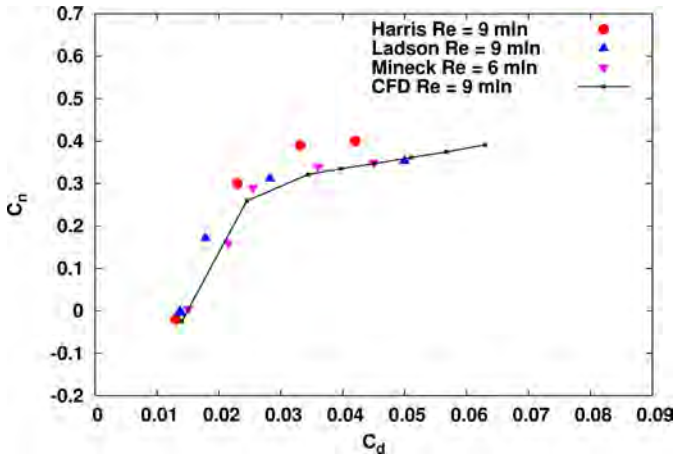

FIG. 21. Normal vs drag force coefficient, $Ma = 0.8$, $Re = 9$ million, $tr = 5\%$, CFD fully turbulent.

Flow conditions with a high Mach number and a relatively low angle of attack creating large supersonic region terminated by the shock wave are a field of interest of the current research. Such conditions are typically found on the advancing blade of the rotor of a helicopter in a high-speed forward flight. The cyclic creation and disappearance of the shock structure due to different relative inflow velocity in every azimuthal position of the blade generates a very strong noise.

We have proven that our numerical method is capable of predicting a flow past the transonic NACA 0012 airfoil with different inflow conditions often found on the helicopter rotor blade.

6. Transonic flow past the NACA 0012 airfoil with a full-chord perforation – validation of the new boundary condition of the perforated wall

The experimental data of Mineck, presented in the previous section, includes a very interesting part related to the tests of the NACA 0012 airfoil with a full-chord porosity. It is very useful in a validation process of the new boundary condition of a perforated wall. This time the porosity p of the upper surface of the airfoil is not constant, but a function of the position on the profile x according to relation:

$$p = 0.0244\sqrt{\sin(\pi x/c)}. \tag{6.1}$$

The porosity is zero at the leading and at the trailing edge, having a maximum value at 50% of the chord length. The mean value of porosity is approximately 1.1%, with a maximum value of 2.44%. The perforation holes have a diameter of 0.254 mm. During calibration of the B/D transpiration model in the Euroshock experiments, the perforation holes diameter was between 0.085 mm and 0.325 mm, with the porosity in the range between 2% and 27%. The perforation value and diameter of holes used in the Mineck experiment fall into this range for the majority of the profile lengths. Only at the leading and trailing edge, the porosity value is so low that it lies outside the bounds of the Euroshock B/D model. Because in this region transpiration velocity is very small due to small values of the porosity, the influence on the flow behaviour should be limited.

It is worth mentioning that the B/D law in the form presented in this paper (Eq. (2.1)) may only be used for certain flow conditions. It was proven experimentally that only at the inlet side of the plate there is an influence of the shear stress in the tangential stream on the transpiration. In a standard passive control, investigated in the Euroshock project, there is a blowing from the cavity in front of the shock and a suction downstream of the shock, if the perforation is placed symmetrically under the shock (Fig. 2). Downstream of the shock usually

a separation region is located, with almost zero shear stress at the wall. It results in a very small influence of the tangential stream on the transpiration velocity. However, the perforation used in the Mineck experiment covers the whole airfoil surface resulting in appearance of the suction also near the leading edge of the profile, in the region of non-zero shear stress. It is believed that due to low values of porosity and small transpiration in this area, the errors introduced by application of B/D law, in a form neglecting shear stress at the wall, are very small.

The inflow Mach number is equal to $Ma = 0.8$, but the Reynolds number is significantly lower, $Re = 4$ million. The angle of attack covered by the experiment and CFD is between $\alpha = -1^\circ$ and $\alpha = 6^\circ$. The transition is again fixed at 5% of the chord in both experiment and computation. The application of a steady state computation to such large angles of attack may be difficult due to the natural movement of the shock (buffeting). However, the comparison of the normal force coefficient C_n between experiment and CFD reveals a very good matching. It is true for both configurations, without and with passive control, even for the highest angle of attack $\alpha = 6^\circ$ (Fig. 22).

On the other hand, the drag force coefficient C_d deviates from the experimental values for both the solid wall and passive control cases, with increasing angle of attack (Fig. 23). For low angles of attack, below $\alpha = 3^\circ$, this deviation is very small, but for the highest angle of attack of $\alpha = 6^\circ$ this discrepancy reaches 20 %. It is worth mentioning that for a certain angle of attack ($\sim \alpha = 1.5^\circ$) crossing of both drag curves is present in both, experiment and CFD, indicating that the profile with perforation exhibits smaller total drag for angles of attack larger than $\alpha = 2^\circ$ that the profile without perforation. This is an interplay between three major contributions: the lower wave losses associated with weaker

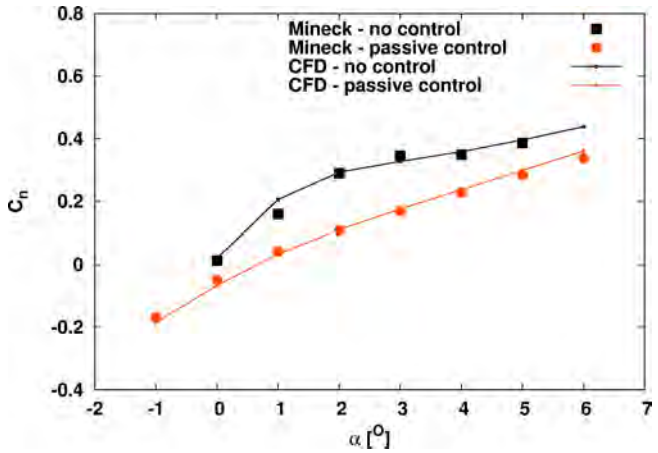

FIG. 22. Normal force coefficient, $Ma = 0.8$, $Re = 4$ million, $tr = 5\%$.

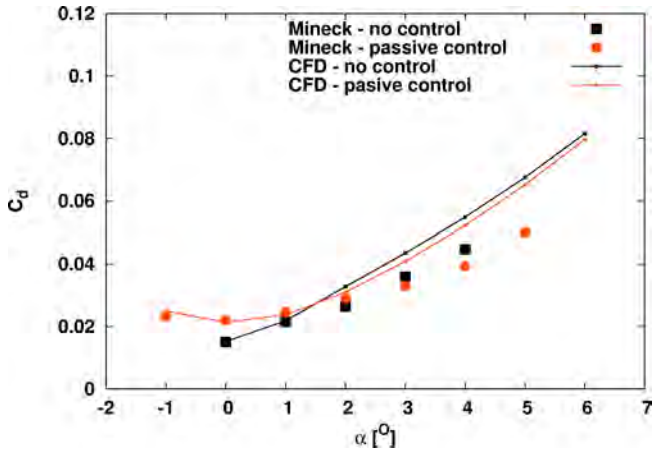

FIG. 23. Drag force coefficient, $Ma = 0.8$, $Re = 4$ million, $tr = 5\%$.

shocks, the decrease of pressure drag connected with a drop of the normal force coefficient and an increase of the viscous drag due to presence of perforation and increased roughness. All these contributions result in a decrease of drag for a given angle of attack for $\alpha > 1.5°$.

For a profile without a perforation the pitching moment coefficient C_m represents the same level of agreement with the experimental data as in the previous computation with $Re = 9$ million (Fig. 24). When a perforation is applied the shape of the moment curve is reproduced very well, but the values tend to deviate from the experimental data. This fact suggests caution when describing the influence of perforation on the pitching moment behaviour of the airfoil without any experimental data available.

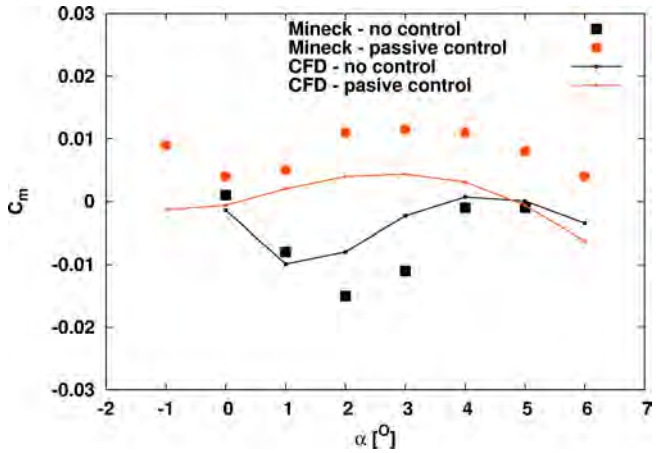

FIG. 24. Pitching moment coefficient, $Ma = 0.8$, $Re = 4$ million, $tr = 5\%$.

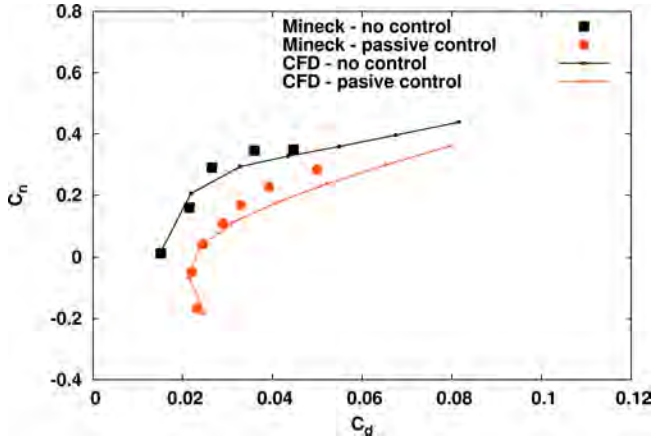

FIG. 25. Normal vs drag force coefficient, $Ma = 0.8$, $Re = 4$ million, $tr = 5\%$.

To illustrate the flow-field and shock system Mach number distributions are presented in Figs. 26, 27 and 28 for angles of attack of $\alpha = 2^\circ$ and $\alpha = 5^\circ$ without and with passive control. The supersonic region is separated by a cut-off at $Ma = 1.0$ of contour lines of Mach number. When a perforation is applied the transpiration velocity is drawn at the plate showing the intensity and direction of the transpiration flow.

The reference shock structure for $\alpha = 2^\circ$ without control is depicted in Fig. 26. The normal shock wave is very strong, having a large height and causing a strong separation of the boundary layer reaching down to the trailing edge. This case is of high importance, because it leads to the generation of a high-speed impulsive noise when it appears on the rotor blade of a helicopter.

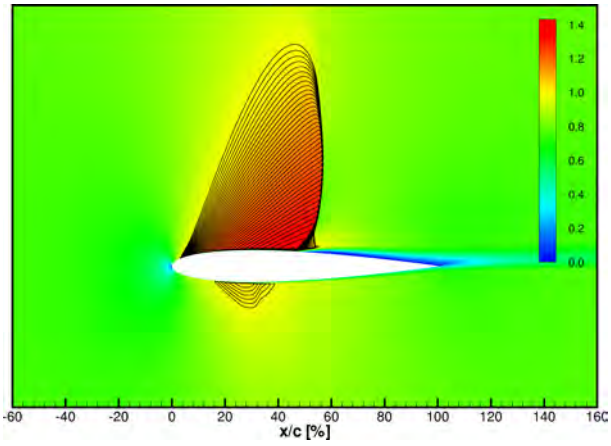

FIG. 26. Contour map of Mach number – no control, CFD, $Ma = 0.8$, $Re = 4$ million, $\alpha = 2^\circ$, $tr = 5\%$.

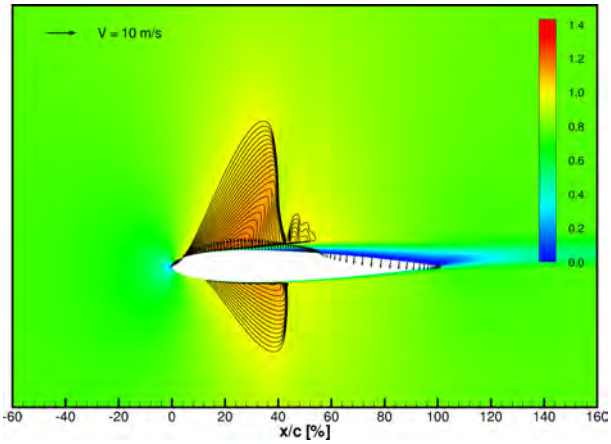

FIG. 27. Contour map of Mach number – passive control, CFD, $Ma = 0.8$, $Re = 4$ million, $\alpha = 2^\circ$, $tr = 5\%$.

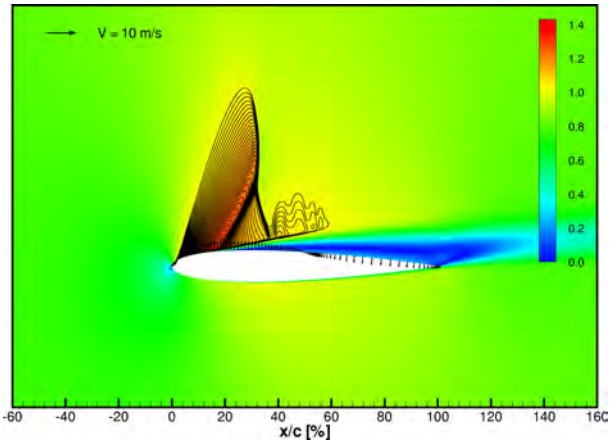

FIG. 28. Contour map of Mach number – passive control, CFD, $Ma = 0.8$, $Re = 4$ million, $\alpha = 5^\circ$, $tr = 5\%$.

The application of the full-chord perforation changes the shock structure significantly (Fig. 27). The conditions on the airfoil result in a small suction into the cavity through the leading edge and a much larger suction in the downstream part of the profile. Significant blowing exists in front of the main shock, causing a generation of the compression waves that weaken the main shock. As a result, the shock system is much smaller with a reduced strength of the main shock.

Unfortunately, the application of passive control decreases the normal force by a factor of 2.5 and increases the drag slightly. To keep the normal force

constant we can increase the angle of attack up to $\alpha = 5°$. This situation is presented in Fig. 28. The change of angle of attack increases acceleration over the forward part of the airfoil, resulting in a larger height of the supersonic region and increased, clearly visible λ-foot structure. The normal force coefficient is restored to its original value, but the drag force is increased, almost two times in comparison with a basic airfoil without control (Tables 4, 5).

Table 4. Experiment of Mineck, $Ma = 0.8$, $Re = 4$ million, $tr = 5\%$.

$\alpha\,[°]$	passive control	C_n	C_d	C_m
2.0	no	0.290	0.0265	−0.015
2.0	yes	0.108	0.0290	0.011
5.0	yes	0.283	0.0500	0.008

Table 5. CFD, $Ma = 0.8$, $Re = 4$ million, $tr = 5\%$.

$\alpha\,[°]$	passive control	C_n	C_d	C_m
2.0	no	0.29352	0.03279	−0.00796
2.0	yes	0.11044	0.03101	0.00397
5.0	yes	0.29475	0.06523	−0.00061

Figures 29 and 30 present a comparison of the measured distribution of the pressure coefficient C_P at the wall with predicted values for all four cases: $\alpha = 2°$ and $\alpha = 5°$, without and with passive control. The shock location for both angles of attack without control is missed by no more than 2% of the chord length. Overall agreement with experimental data is good enough, especially in the presence of perforation.

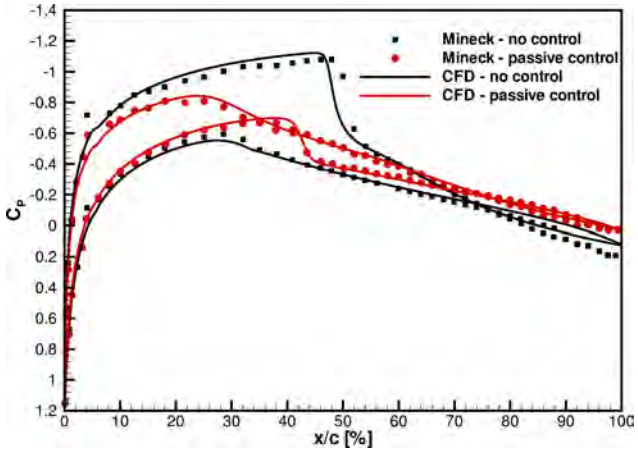

FIG. 29. C_p distribution at the wall, $Ma = 0.8$, $Re = 4$ million, $\alpha = 2°$, $tr = 5\%$.

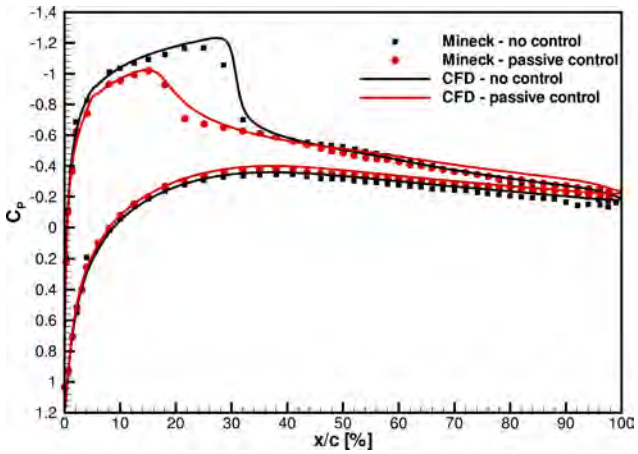

FIG. 30. C_p distribution at the wall, $Ma = 0.8$, $Re = 4$ million, $\alpha = 5^\circ$, $tr = 5\%$.

It was proven that our numerical method is capable of predicting a flow past the transonic NACA 0012 airfoil equipped with a full-chord perforation. The details of the influence of transpiration flow are captured well enough to constitute application of our code in the research focused on the disintegration of the shock wave by application of the passive cavity covered with a perforated plate with a properly designed location, length and porosity.

7. Transonic flow past the NACA 0012 airfoil with a 60% of the chord length perforation – influence of porosity value 2.5%, 5% and 10%

At the beginning of the purely numerical research we have applied different perforation lengths (25% c, 35% c, 45% c and 60% c) to the NACA 0012 profile to disintegrate the shock using flow conditions from Sec. 5 ($Ma = 0.8$, $Re = 9$ million and $\alpha = 2.26^\circ$) and porosity of 5%, but without a prescribed transition location – computations were fully turbulent. The most effective length of the perforation was chosen to be 60% c located between 20% and 80% of the chord length. In this paper only the results obtained for a perforation length of 60% c are presented.

In order to optimise the method it was necessary to check the influence of the porosity value on effectiveness of the 60% c perforation in disintegration of the shock. The influence of a porosity value, in form of Mach number contour maps, is presented in Figs. 31, 32 and 33. Here each porosity value out of 2.5%, 5% and 10% generates different transpiration flow through the plate and individual shock structure.

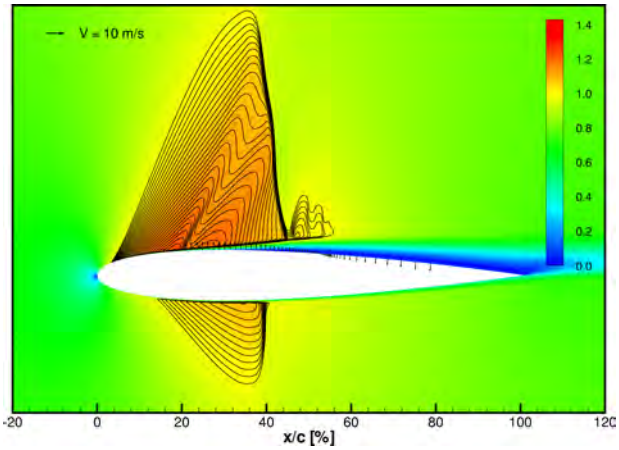

FIG. 31. Contour map of Mach number, porosity 2.5%, CFD, $Ma = 0.8$, $Re = 9$ million, $\alpha = 2.26^\circ$, fully turbulent.

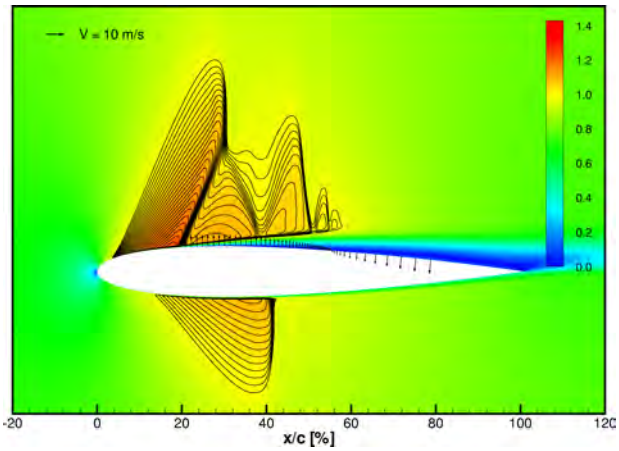

FIG. 32. Contour map of Mach number, porosity 5%, CFD, $Ma = 0.8$, $Re = 9$ million, $\alpha = 2.26^\circ$, fully turbulent.

The porosity value of 2.5% results in a very small transpiration velocity (Fig. 31). It causes generation of only slight oblique compression wave at the beginning of the plate intersecting normal shock. The main shock remains strong. On the other hand, application of the 10% porosity leads to a very strong transpiration (Fig. 33). The flow is disturbed so much, that the whole compression is located upstream of the beginning of the perforated plate. Only the medium value of porosity 5% leads to a desired change of the structure of the shocks, from a single normal shock wave to the system of compressions reflecting between the surface of the airfoil and the edge of the supersonic region (Fig. 32).

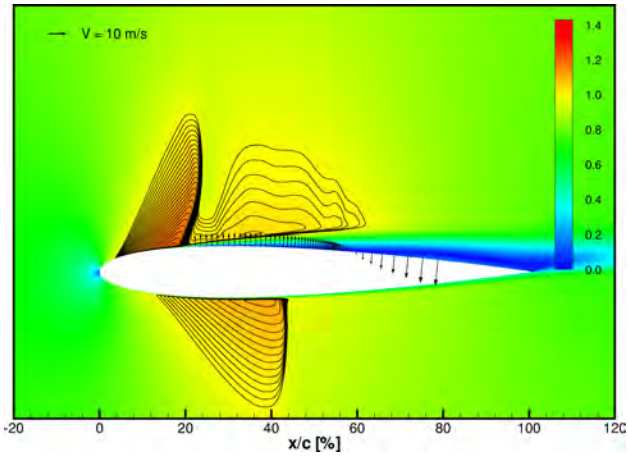

FIG. 33. Contour map of Mach number, porosity 5%, CFD, $Ma = 0.8$, $Re = 9$ million, $\alpha = 2.26°$, fully turbulent.

The aerodynamic coefficients for all three porosities, and for a clean airfoil, are summarized in Table 6. It can be observed that the application of a perforated plate of 5% porosity leads to a decrease of the normal force coefficient by the factor of 2.5, keeping drag below the basic value.

Table 6. ***Ma* = 0.8, *Re* = 9 million, $\alpha = 2.26°$, perforation location 20% c – 80% c.**

porosity [%]	C_n	C_d	C_m
0.0	0.32107	0.03437	−0.00959
2.5	0.15802	0.02986	0.00659
5.0	0.12796	0.03095	0.00381
10.0	0.10272	0.03263	−0.00151

As a result of this investigation, it is proposed (for the given flow conditions) to disintegrate the shock wave by application of a passive control in the form of perforation of the length of 60% c and the porosity value of 5%. The passive cavity should be located between 20% and 80% of the chord length.

8. Disintegration of the shock wave on the NACA 0012 airfoil with a 60% of the chord length perforation

In order to use passive control, a method of a restoration of the normal force coefficient has to be proposed. The advancing blade of a helicopter rotor in a high-speed forward flight has enough normal force even for a very low angle

of attack (usually 2°–3° on the advancing side of a rotor), which may be easily increased. It is proposed to correct the angle of attack after applying perforation to match the normal force coefficient without passive control.

The correction of angle of attack has to be large to obtain the same normal force coefficient as that without perforation. However, on a helicopter blade only the outer part should be subjected to passive control where shock systems are generated. It means that there would be still a large part of the blade which, when perforation is applied, will not exhibit any loss of lift. It means that a restoration of the thrust coefficient C_t of the rotor will require a much smaller correction of the angle of attack of a whole blade in comparison with an airfoil.

The potential of the 60% perforation in disintegration of the shock wave is limited by a need to restore a proper normal force coefficient. It is required to predict the flow behaviour in presence of passive control for higher angles of attack necessary to obtain similar normal force coefficients comparable with no control case. In Figs. 34, 35, 36 and 37 the computed aerodynamic characteristics of the NACA 0012 profile without control and with perforation of 60% of the chord length (5% porosity) are presented. Flow conditions are again $Ma = 0.8$, $Re = 9$ million and no transition. Angle of attack is increased from the basic $\alpha = 2.26°$ up to $\alpha = 5.26°$ to obtain (in presence of a perforation) a normal force coefficient value equal to the value without control. It is evident that correction of the angle of attack equal to 3° is necessary to keep the profile at the same normal force coefficient (Table 7). With this correction the drag force coefficient is increased almost twice, leaving a very large space for improvement. On the other hand, application of the cavity with a perforated plate can have a positive effect on the pitching moment coefficient – for the whole range of angles of attack its value is substantially reduced.

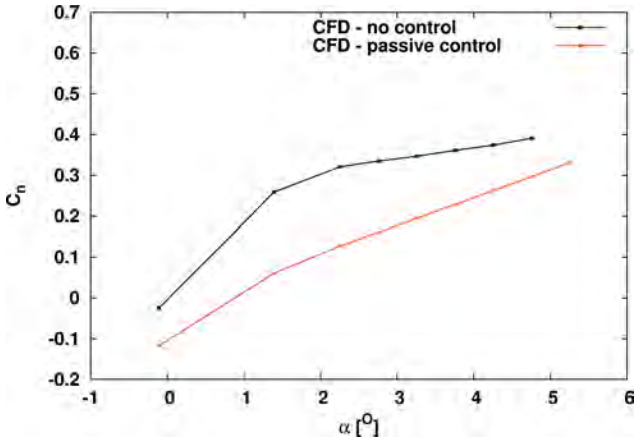

FIG. 34. Normal force coefficient, $Ma = 0.8$, $Re = 9$ million.

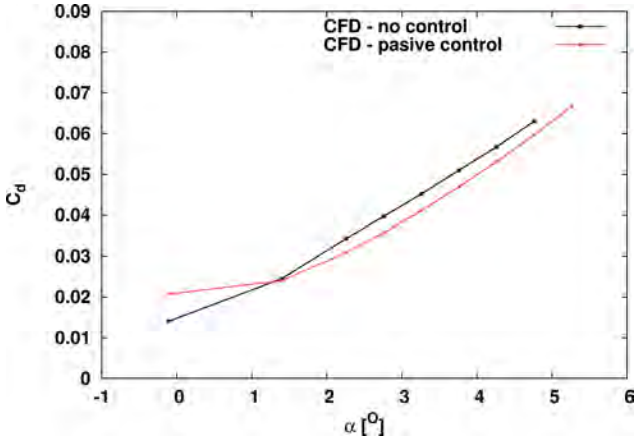

FIG. 35. Drag force coefficient, $Ma = 0.8$, $Re = 9$ million.

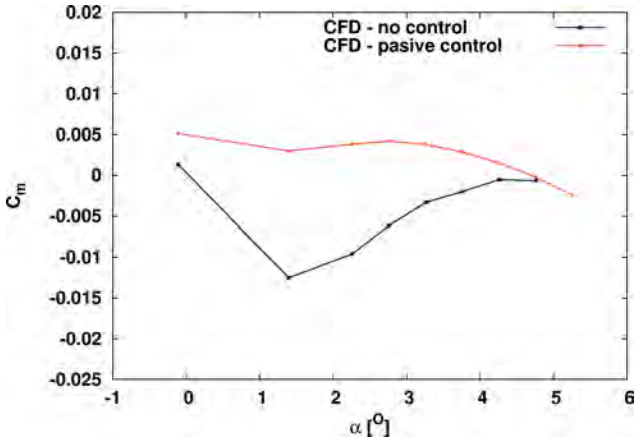

FIG. 36. Pitching moment coefficient, $Ma = 0.8$, $Re = 9$ million.

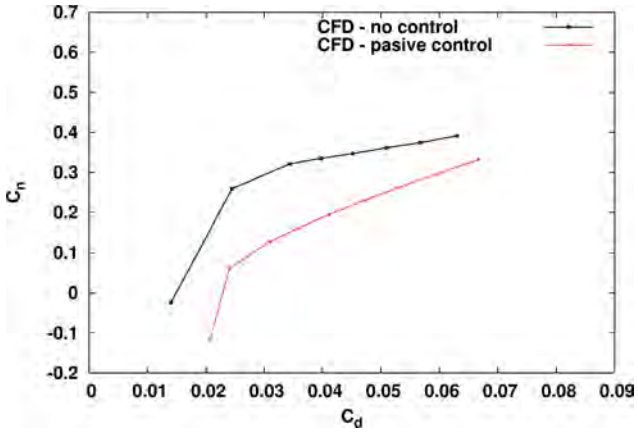

FIG. 37. Normal vs drag force coefficient, $Ma = 0.8$, $Re = 9$ million.

Table 7. CFD, $Ma = 0.8$, $Re = 9$ million, fully turbulent, perforation location 20% – 80% c.

α [°]	passive control	C_n	C_d	C_m
2.26	no	0.32107	0.03437	−0.00959
2.26	yes	0.12796	0.03095	0.00381
5.26	yes	0.33138	0.06664	−0.00242

To visualize the flow field and shock structure contour maps of the Mach number are presented in Figs. 38, 39 and 40 for all three considered cases. By application of the perforation, a strong, normal shock wave (Fig. 38) is disinte-

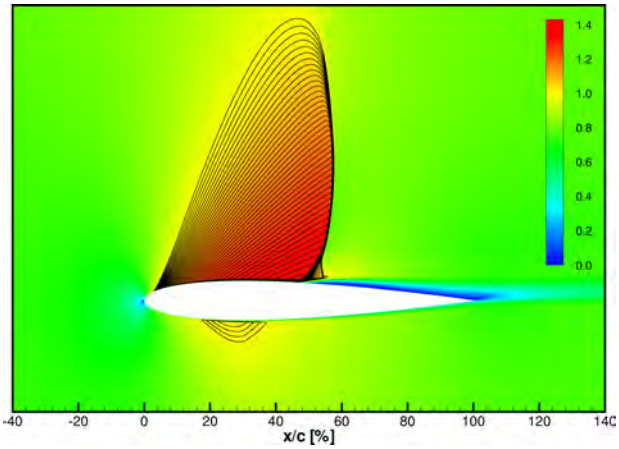

FIG. 38. Contour map of Mach number – no control, CFD, $Ma = 0.8$, $Re = 9$ million, $\alpha = 2.26°$, fully turbulent.

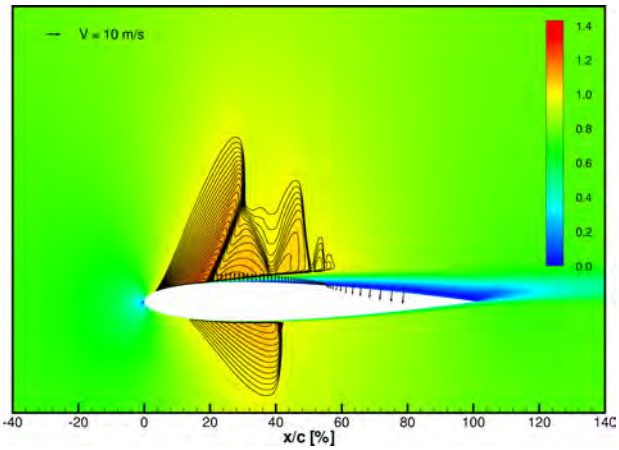

FIG. 39. Contour map of Mach number – passive control, CFD, $Ma = 0.8$, $Re = 9$ million, $\alpha = 2.26°$, fully turbulent.

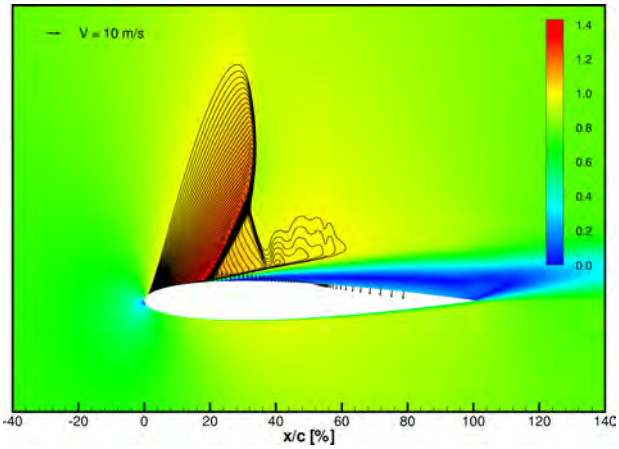

FIG. 40. Contour map of Mach number – passive control, CFD, $Ma = 0.8$, $Re = 9$ million, $\alpha = 5.26°$, fully turbulent.

grated into a compression wave that is reflecting between a boundary layer and a sonic line (Fig. 39). Correction of the angle of attack necessary to restore the normal force coefficient value without control, again changes the topology of the shock system into a very large λ-foot (Fig. 40). The efficiency of this method is strictly connected with the value of the correction of the angle of attack necessary to keep a normal force on the desired level. Even for this high angle of attack, the height and length of the supersonic region are reduced, revealing the potential for noise reduction associated with the shocks.

The influence of perforation on the distribution of the pressure coefficient C_P on the surface of the airfoil is presented in Fig. 41. The passive cavity smears the pressure gradient at the wall ($\alpha = 2.26°$), the maximum Mach number in front of the shock is reduced together with an extent of the supersonic flow. Even when a correction of the angle of attack is applied ($\alpha = 5.26°$), the dimensions of the supersonic region are reduced. Unfortunately, the maximum Mach number value is comparable with the basic flow without control.

The effectiveness of the method may be judged also by the analysis of the total pressure losses associated with the viscous effects and shock waves. In Fig. 42 a total pressure profile downstream of the airfoil is presented. Two distinct areas may be pointed out; the main area of viscous losses in the wake of an airfoil and the region of wave losses connected with strong shocks just above a wake. Both effects are clearly visible in the total pressure profile for flow without control ($\alpha = 2.26°$). Application of passive cavity increases viscous losses slightly, reducing the shock losses almost completely ($\alpha = 2.26°$). Correction of the angle of attack again leads to large total viscous pressure losses, with only a small neg-

ative effect on wave drag ($\alpha = 5.26°$). The prosposed method is very effective in reduction of the wave drag associated with strong shocks leading to smaller total pressure losses in the area behind a shock, above the boundary layer edge.

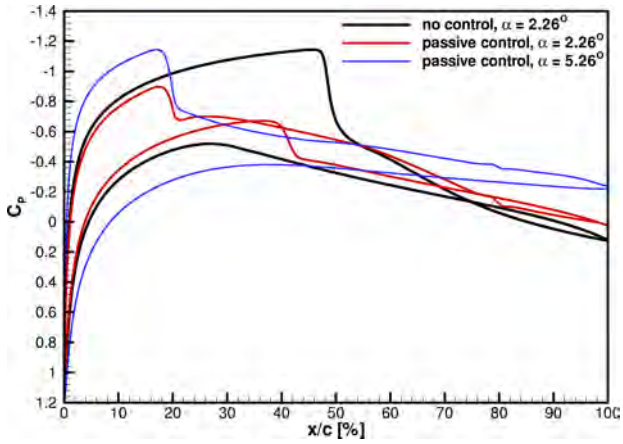

FIG. 41. C_p distribution at the wall, CFD, $Ma = 0.8$, $Re = 9$ million, fully turbulent.

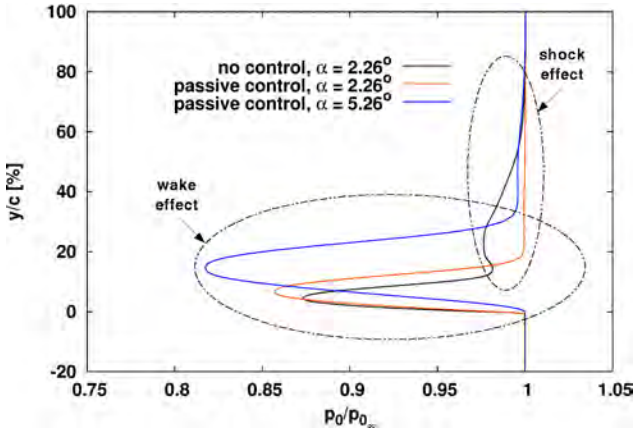

FIG. 42. Wake profile 95.25 % c downstream of the trailing edge, CFD, $Ma = 0.8$, $Re = 9$ million, fully turbulent.

From the acoustic point of view, the most important sources of noise are rapid pressure changes on shock waves located above the wall, not smoothed by the presence of a boundary layer. To visualize the influence of perforation on this source of noise pressure distributions above the wall are presented again for all three cases in Figs. 43, 44 and 45. Three locations are chosen (0.1 c, 0.4 c and 0.7 c) above the surface of the airfoil to visualise static pressure changes.

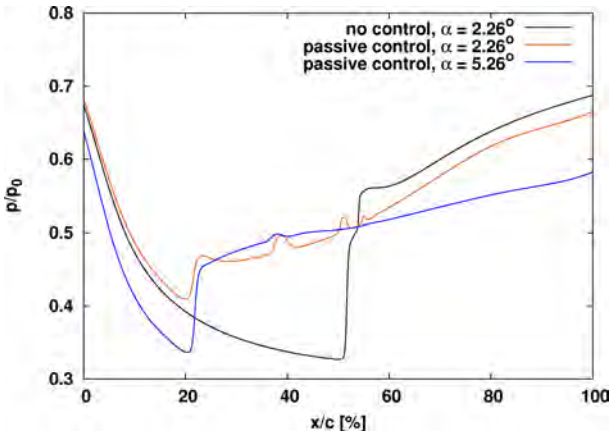

FIG. 43. Pressure distribution at $y = 0.1\ c$, CFD, $Ma = 0.8$, $Re = 9$ million, fully turbulent.

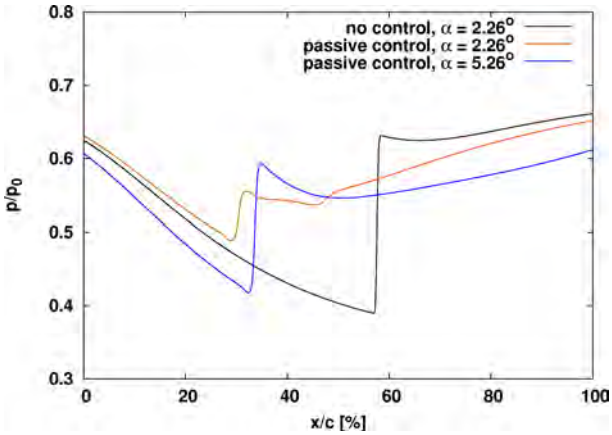

FIG. 44. Pressure distribution at $y = 0.4\ c$, CFD, $Ma = 0.8$, $Re = 9$ million, fully turbulent.

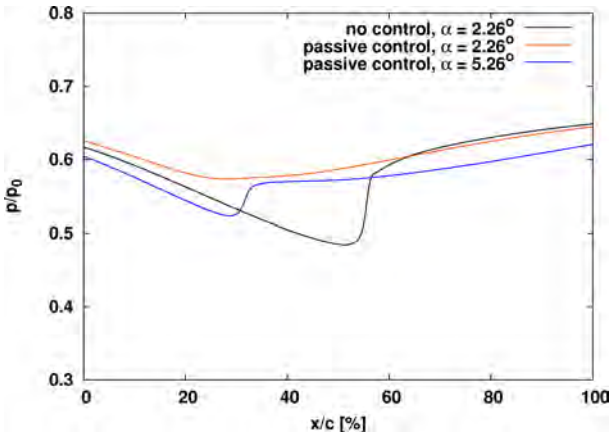

FIG. 45. Pressure distribution at $y = 0.7\ c$, CFD, $Ma = 0.8$, $Re = 9$ million, fully turbulent.

The flow without passive control exhibits the largest static pressure gradients above the wall (black lines). All three cross-sections present a strong shock near 50% of the chord length of the airfoil ($\alpha = 2.26°$). Flow control in the form of a passive cavity changes this picture significantly (red lines). All pressure gradients observed are smoothed out almost completely ($\alpha = 2.26°$). This is an evidence that by this method, a source of a high-speed noise can be dramatically reduced. Unfortunately, the correction of the angle of attack leads to the increase of the value of pressure gradients ($\alpha = 5.26°$). It is worth mentioning that the original, very high jump of pressure is nevertheless much smaller (blue lines). Resulting picture of the flow gradients above the wall has only half of the strength of the original, strong shock distribution (Fig. 43).

These data suggest that the proposed methodology may be efficiently applied to disintegrate the shock on a transonic airfoil. It is very effective in reduction of the pressure gradients associated with shocks, the main source of a high-speed impulsive noise. However, this method can lead to a substantial reduction of the normal force accompanied by a reduction of total drag. When too much correction is applied to the angle of attack to restore the lift, an excessive value of drag is produced.

9. Conclusions

Numerical results confirm that the implementation of the B/D transpiration flow model into the SPARC code has been performed correctly. The calculated flow in the curved nozzle equipped with a perforation and past the NACA 0012 transonic airfoil with passive cavity, agrees well enough with the experimental data to validate the new boundary condition.

The CFD analysis of a new phenomenon of the shock disintegration confirms the applicability of this type of passive control to the reduction of a high-speed impulsive noise. The CFD method used proved to be correct and may be used with confidence for many applications of the transpiration flow.

In the particular case of rotor aerodynamics, the correction applied to the angle of attack does not request full regain of the lift because the transonic flow takes place only at the tip of the blade. Therefore, the disintegration of the shock system by passive control will require only a slight increase of the angle of attack, resulting in a substantial reduction of the high-speed impulsive noise.

References

1. E. Stanewsky, J. Delery, J. Fulker, W. Geissler, *EUROSHOCK: drag reduction by passive shock control; results of the project EUROSHOCK, AER 2-CT92-0049 supported by the European Union 1993–1995*, Vieweg, Braunschweig 1997.

2. E. STANEWSKY, J. DELERY, J. FULKER, P. MATTEIS, *Drag reduction by shock and boundary layer control: results of the project EUROSHOCK II supported by the European Union 1996-1999*, Springer-Verlag, Berlin 2002.

3. F. MAGAGNATO, *"Kappa" – Karlsruhe parallel program for aerodynamics*, TASK Quarterly, **2**, 2, 215–270, 1998.

4. P. DOERFFER, R. BOHNING, *Modelling of perforated plate aerodynamics performance*, Aerospace Science and Technology, **4**, 525–534, 2000.

5. P. DOERFFER, R. BOHNING, *Shock wave – boundary layer interaction control by wall ventilation*, Aerospace Science and Technology, **7**, 171–179, 2003.

6. W. BRAUN, *Experimentelle Untersuchung der turbulenten Stoß-Grenzschicht-Wechselwirkung mit passiver Beeinflussung*, PhD thesis, Karlsruhe, 1990.

7. T. L. HOLST, *Viscous transonic airfoil workshop compendium of results*, Journal of Aircraft, **25**, 12, 1073–1087, 1988.

8. C. D. HARRIS, *Two-dimensional aerodynamic characteristics of the NACA 0012 airfoil in the Langley 8-foot transonic pressure tunnel*, NASA Technical Memorandum 81927, 1981.

9. C. L. LADSON, A. S. HILL, W. G. JOHNSON JR., *Pressure distributions from high Reynolds number transonic tests of an NACA 0012 airfoil in the Langley 0.3-meter transonic cryogenic tunnel*, NASA Technical Memorandum 100526, 1987.

10. C. L. LADSON, A. S. HILL, *High Reynolds number transonic tests of an NACA 0012 airfoil in the Langley 0.3-meter transonic cryogenic tunnel*, NASA Technical Memorandum 100527, 1987.

11. R. E. MINECK, P. M. HARTWICH, *Effect of full-chord porosity on aerodynamic characteristics of the NACA 0012 airfoil*, NASA Technical Paper 3591, 1996.

Received April 21, 2006; revised version July 10, 2006.